LA-UR-99-6059: *Conference on Recent Advances in Structural Dynamics*, Southampton, UK, July 22-25, 2000.

DAMAGE DIAGNOSIS USING STATISTICAL PROCESS CONTROL

Hoon Sohn[†], Michael L. Fugate[‡], and Charles R. Farrar[†]

Los Alamos National Laboratory
Los Alamos, NM 87545

ABSTRACT

Structural health monitoring is described in the context of a statistical process control paradigm. This paper demonstrates the application of various statistical process control techniques such as the Shewhart, the exponentially weighted moving average, and the cumulative sum control charts to vibration-based damage diagnosis. The control limits are first constructed based on the measurements obtained from the initial intact structure. Then, new data are monitored against the control limits. A statistically significant number of outliers outside the control limits indicate a system transition from a healthy state to a damage state. Environmental and operation conditions, such as temperature change and the magnitude variation of the input forces, are also incorporated into the monitoring process. Blind tests of various damage cases are conducted without prior knowledge of the actual damage scenarios to evaluate the performance of the presented control chart techniques.

1. INTRODUCTION

Many aerospace, civil, and mechanical engineering systems continue to be used despite aging and the associated potential for damage accumulation. Therefore, the ability to monitor the structural health of these systems is becoming increasingly important from both economic and life-safety viewpoints.

This paper attempts to state in a quantifiable manner if the system of interest has experienced structural deterioration or degradation by analyzing changes in the vibration response of the system in the presence of operational, and/or environmental variability. In particular, this paper casts the structural monitoring

[†] Engineering Sciences & Application Division, Engineering Analysis Group, MS C926.
[‡] Computing, Information, & Communications Division, Computer Research & Applications Group, MS B265.

problem in the context of a control chart analysis paradigm, which is one of the most popular methods of statistical process control. The control chart approach is very efficient and suitable for on-line continuous monitoring. The final diagnosis results are presented to end users in three categories: safe (green light), questionable (yellow light), and danger (red light) making the interpretation of the final diagnosis simple.

2. THEORETICAL FORMULATION

An auto-regressive (AR) model is first fitted to the measured acceleration-time histories from an undamaged structure. Residual errors, which quantify the difference between the prediction from the AR model and the actual measured time history at each time interval, are used as the damage-sensitive features. Next, the Shewhat, cumulative sum (CUSUM), and exponentially weighted moving average (EWMA) control charts are employed to monitor the mean and variance of the selected features. Control limits for the control charts are constructed based on the features obtained from the initial intact structure. The residual errors computed from the new data and the prediction of these data with the initial AR model are then monitored against the control limits. A statistically significant number of residual error terms outside the control limits indicate a system anomaly. In this section, the AR modeling, and the construction of the various control charts are briefly explained.

2.1. Modeling of a Auto-Regressive Process

One of the main assumptions in the use of control charts is the independence of the extracted features. Conventional control charts provide false-positive indications of damage too frequently if the selected features exhibit a high level of correlation over time. Therefore, the correlation in the raw time history data needs to be removed prior to the application of the control charts. As a feature extraction process, an AR model is fitted to the time history data in order to remove the correlation. An AR model with p auto-regressive terms can be written:

$$u(k) = a + \sum_{j=1}^{p} \phi_j \, u(k-j) \; + b\mathrm{T} + e(k) \qquad (1)$$

This model is referred to as an AR(p) model. $u(k)$ is the observed time history at time $k\Delta t$, and Δt is a sampling interval. ϕ_j is an unknown auto-regression coefficient, and $e(k)$ is an unobservable random error with zero mean and constant variance. T is some form of a current temperature measure for the system and b is the associated coefficient. The ϕ_j's and b are estimated by fitting the AR model to the data obtained from the undamaged structure. The mean of $u(k)$ for all k is μ and $a \equiv \left(1-\sum \phi_j\right)\mu$.

Denoting $\hat{u}(k)$ as the predicted time history from the AR model at time index k, the residual error, $e(k)=u(k)-\hat{u}(k)$, is defined as the damage sensitive feature to be used in this study. When new data become available, the response at the current time point is predicted using p past time points, current temperature T, and the previously fitted AR(p) model. Then, the residual errors are computed for $k = p+1,\ p+2,\ldots$.

When the system varies from the initial condition and the AR model derived from the undamaged structure is applied to the new data, the AR model will show greater residual errors. However, the variation of the residual errors does not necessarily indicate that the structure is damaged. For example, variations of environmental or operational conditions such as ambient temperature, wind speed, or traffic intensity of *in-situ* bridges could also cause shifts of the residual error distribution. Therefore, the effects of these environmental or operational conditions on residual errors should be first discriminated from the effects of damage.

The measurement of the system's current temperature parameter, T, is incorporated directly in Equation (1) to take into account the effect of temperature variance on the measure response. The response time series are also normalized by the estimated standard deviation of the time series to remove the influence of the input amplitude change. Consequently, the residual error changes caused by damage are separated from the variations caused by the ambient temperature and input force intensity. The following various control charts provide statistical frameworks to detect the changes in the mean and variance of the residuals.

2.2. Shewhart Control Chart

In this section, two most commonly used Shewhart control charts, X-bar and S control charts, are presented. The X-bar control

chart provides a framework for monitoring the changes of the selected feature means and for identifying observation points that are inconsistent with the past data sets. The S control chart monitors the process variance in a similar way as the X-bar control chart. We first introduce the X-bar control chart and then address the S chart.

To monitor the mean variation of the features, the features are first arranged in *m* subgroups of size *n*:

$$\begin{matrix} x_{11} & x_{12} & \cdots & x_{1n} \\ x_{21} & x_{22} & \cdots & x_{2n} \\ \vdots & \vdots & & \vdots \\ \vdots & \vdots & & \vdots \\ x_{m1} & x_{m2} & \cdots & x_{mn} \end{matrix} \tag{2}$$

where x_{ij} is the extracted feature from previous section, *i.e.*, the residual in this study. The subgroup size *n* is often taken to be 4 or 5. If *n* is chosen too large, a drift that may be present in individual subgroup mean may be obscured, or averaged-out. An additional motivation for using the rational subgrouping, as opposed to employing individual observations, is that the distribution of the subgroup means can often be reasonably approximated by a normal distribution as a result of the central limit theorem.

Next, the sample mean $\overline{\mathrm{X}}_i$ and standard deviation S_i of the features are computed for each subgroup ($i = 1, \cdots, m$):

$$\overline{\mathrm{X}}_i = mean\left(x_{ij}\right) \text{ and } \mathrm{S}_i = std(x_{ij}) \tag{3}$$

Here, the calculation of the mean and standard deviation is with respect to the *n* observations in each subgroup. Finally, a control chart is constructed by drawing a centerline (CL) at the mean of the subgroup means and two additional horizontal lines corresponding to the upper and lower control limits (UCL & LCL) versus subgroup numbers (or with respect to time). The centerline and two control limits are defined as follows:

$$\begin{gathered} \mathrm{UCL} = \mathrm{CL} + Z_{\alpha/2}\frac{\mathrm{S}}{\sqrt{n}},\ \mathrm{LCL} = \mathrm{CL} - Z_{\alpha/2}\frac{\mathrm{S}}{\sqrt{n}} \\ \text{and } \mathrm{CL} = mean(\overline{\mathrm{X}}_i) \end{gathered} \tag{4}$$

where the calculation of mean is with respect to all subgroups ($i = 1, \cdots, m$). $Z_{\alpha/2}$ represents the $\alpha/2$ quantile of the standard normal

distribution. The variance S^2 is estimated by averaging the variance S_i of all subgroups:

$$S^2 = mean(S_i^2) \tag{5}$$

As mentioned before, regardless of the distribution of x_{ij}, $\overline{X}_i$ can be approximated by a normal distribution as a result of the central limit theorem. Therefore, the control limits in Equation (4) correspond to a $100(1-\alpha)\%$ confidence interval. In many practical situations, the distribution of features may not be exactly normal. However, it has been shown that the control limits based on the normality assumption can often be successfully used unless the population is extremely non-normal [6]. The observation of the residual errors obtained from the undamaged structure reveals that the normaltiy assumption is an appropriate approximation for this study.

If the system experiences damage, this will likely be indicated by an unusual number of subgroup means outside the control limits (a charted value outside the control limits is referred to as an *outlier* in this paper). Finally, damage monitoring is performed by plotting the $\overline{X}_i$ values obtained from the new data set along with the previously constructed control limits.

Similar to the X-bar control chart, the variance of the individual subgroups, S_i, can be monitored by the S control chart. To construct the S control chart, UCL, LCL, and CL are defined as follows:

$$\text{UCL} = S\sqrt{\frac{\chi^2_{1-\alpha/2,n-1}}{n-1}},\ \text{LCL} = S\sqrt{\frac{\chi^2_{\alpha/2,n-1}}{n-1}} \text{ and } \text{CL} = mean(S_i) \tag{6}$$

where $\chi^2_{1-\alpha/2,\,n-1}$ and $\chi^2_{\alpha/2,\,n-1}$ denote the upper and lower percentage points of the chi-square distribution with $n-1$ degrees of freedom.

2.3. Cumulative Sum Chart

The X-bar and S control charts use only the information contained in the current point and ignore any information given by the entire sequence of points. This feature makes the X-bar and S control charts relatively insensitive to small shifts in the process. Alternatives to monitor more subtle changes are the CUSUM and EWMA control charts. First, the CUSUM control chart is presented here.

The CUSUM chart incorporates all the previous information up to the current point by accumulating the deviations of the feature

values from the centerline. However, the CUSUM chart for the process mean is formed by computing the following cumulative sum:

$$C_i = \sum_{j=1}^{i} \left(\overline{X}_i - CL \right) \tag{7}$$

Note that if the sample mean $\overline{X}_i$ remains in control around the CL value, the cumulative sum C_i defined in Equation (7) should be a random process with zero mean. For example, if the process mean shifts upward to a new mean value, say $CL^+ > CL$, then a positive drift in the cumulative sum C_i will be accumulated. Similarly, the downward shift of the process mean will develop a negative drift in C_i. Therefore, a trend developed among observations is utilized as an indication of the process mean shift. Since the CUSUM includes all the information up to and including the *i*th point, the CUSUM is more effective than the Shewhart charts for detecting small shifts. Particularly, the CUSUM are effective with subgroup size one ($n = 1$).

The actual CUSUM chart is implemented by accumulating upward and downward derivation from the CL separately:

$$\begin{aligned} C_i^+ &= \max[0,\ \overline{X}_i - (CL + K) + C_{i-1}^+] \\ C_i^- &= \max[0,\ (CL - K) - \overline{X}_i + C_{i-1}^-] \end{aligned} \tag{8}$$

where C_0^+ is the upper cumulative sum of derivations that are above CL + K, and C_0^- is the lower cumulative sum of derivations that are below CL - K. Note that the starting values are $C_0^+ = C_0^- = 0$ and both C_0^+ and C_0^- are reset to zero upon becoming negative. The reference value (or allowance value) K in Equation (8) is often set about one half of the deviation that one is interested in detecting. For example, if we intend to detect one standard deviation shift from the target value, K is chosen to be one-half of the standard deviation, $K = \sigma/2$. When either C_0^+ or C_0^- exceed the decision interval H, the process is out of control. H is often defined to be five times the standard deviation σ, H=5σ [6].

Similarly, a CUSUM chart for monitoring process variance can be formulated. Denoting $Y_i = (\overline{X}_i - CL)/\sigma$ and a standardized quantity V_i as follows

$$V_i = \frac{\sqrt{|Y_i|} - 0.822}{0.349} \tag{9}$$

Hawkins (1981) [3] shows that the in-control distribution of V_i is approximately a normal distribution with zero mean and unit standard deviation. Then, two one-sided CUSUMs for process variance can be defined as follows:

$$\begin{aligned} S_i^+ &= \max[0,\ V_i - K + S_{i-1}^+] \\ S_i^- &= \max[0,\ -K - V_i + S_{i-1}^-] \end{aligned} \tag{10}$$

where $S_0^+ = S_0^- = 0$, and the values for K and H are selected as in the case of the process mean monitoring.

2.4. Exponentially Weighted Moving-Average Control Chart

The EWMA chart is also a good alternative to the Shewhart charts for detecting small shifts [4,7]. The performance of the EWMA is often equivalent to that of the CUSUM chart. When a subgroup size is one ($n = 1$), the EWMA chart is defined as:

$$z_i = \lambda x_i + (1-\lambda) z_{i-1} \tag{11}$$

where λ is a constant with $0 < \lambda \leq 1$, and the starting value z_0 is the target mean, $z_0 = \mathrm{CL}$. Recursively substituting $\lambda x_{i-j} + (1-\lambda) z_{i-j-1}$ for z_{i-j}, $j = 1, 2, ..., i-1$, in Equation (11), it can be shown that z_i is a weighted average of all past and current observations:

$$z_i = \lambda \sum_{j=0}^{i-1} (1-\lambda)^j x_{i-j} + (1-\lambda)^i z_0 \tag{12}$$

If the observations x_i are independent random variables with variance σ^2, the variance of z_i becomes:

$$\sigma_{z_i}^2 = \sigma^2 \left(\frac{\lambda}{2-\lambda} \right) [1 - (1-\lambda)^{2i}] \tag{13}$$

Finally, the control limits and center line for the EWMA are defined as

$$\mathrm{UCL, LCL} = \mathrm{CL} \pm L\sigma \sqrt{\frac{\lambda}{(2-\lambda)} [1 - (1-\lambda)^{2i}]} \tag{14}$$

and $\mathrm{CL} = mean(x_i)$. Note that, since z_i is a weighted sum of all past and current observations, the distribution of z_i can be reasonably approximated by a normal distribution as a result of the central limit

theorem. Therefore, the EWMA chart is insensitive to the normality assumption of individual observations x_i.

In Equation (14), L and λ are the design parameters of the EWMA chart. In this study, the values of L and λ are chosen L=2.7 and λ=0.1 to give approximately the same confidence interval as that of the CUSUM chart with $K = \sigma/2$ and H=5σ [6].

MacGregor and Harris (1993) extended the use of EWMA-based statistics for monitoring the process variance [5]. The exponentially weighted moving variance (EWMV) is defined as:

$$s_i^2 = \lambda (x_i - z_i)^2 + (1-\lambda)\, s_{i-1}^2 \qquad (15)$$

It can be shown that $E[s_i^2] = \sigma^2$, and z_i is an estimate of the true population mean at the *i*th point in time. If individual observations are independent, the s_i^2 approximately has chi-square distribution with $v = (2-\lambda)/\lambda$ degrees of freedom. Finally, the control limits for $\sqrt{s_i^2}$ statistic become:

$$\text{UCL} = \sigma \sqrt{\frac{\chi^2_{1-\alpha/2,v}}{v}} \text{ and } \text{LCL} = \sigma \sqrt{\frac{\chi^2_{\alpha/2,v}}{v}} \qquad (16)$$

All the control charts are constructed such that the control limits approximately correspond to a 99% confidence interval of the given distribution.

3. APPLICATIONS

The applicability of the aforementioned control charts to damage diagnosis problems is demonstrated using the vibration test data simulated from the spring-mass system shown in Figure 1. The springs act in the axial direction and have nominal values of k_o = 1x10^7 N/m. The masses have a nominal value of m_o = 1.0 N-S^2/m and nominal damping of the dashpots is c_o = 5%. In Figure 1, the spring, dashpot, and mass elements are numbered from left to right, k1-k11, c1-c11, m1-m10, respectively.

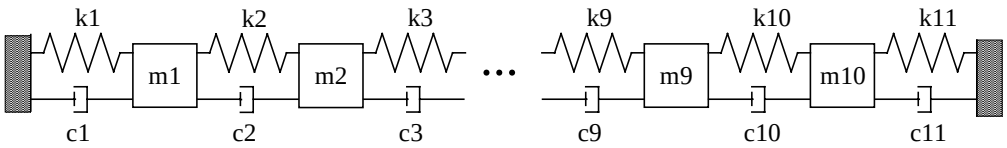

Figure 1: A spring-mass system

Excitation time series is generated such that it has a flat spectrum up to a cutoff frequency of 512 Hz. For all cases, the input force is applied at m9. One of the requirements of this study is the ability to input environmental variability into the system. The spring constant is designed to be a nonlinear function of temperature as shown in Figure 2. In this figure, the spring stiffness had a nominal value of $1x10^7$ N/m at a temperature of 15^o C. Then, a maximum variance of ±2.5% over a temperature range of -10^o to 40^o C is assigned.

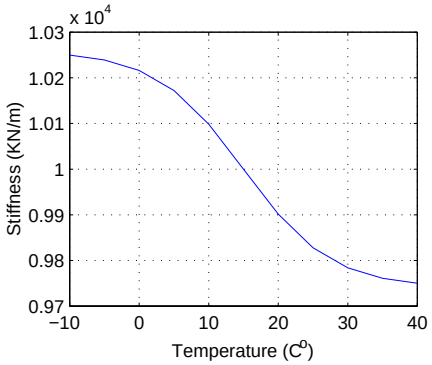

Figure 2: Temperature-stiffness relationship

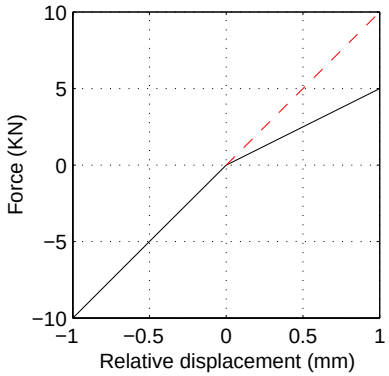

Figure 3: Damage simulation using a bilinear stiffness model

Nonlinear damage is introduced to the structure by reducing the stiffness of a spring in tension side. Therefore, after damage occurrence, the spring will have a bilinear force-displacement relationship as shown in Figure 3. In subsequent examples, the amount of damage is denoted by the percentage decrease of the tensional stiffness. For example, the stiffness in compression is $1x10^7$ N/m and in tension it is $5x10^6$ N/m for Figure 3 denoting 50% stiffness decrease.

Table 1 shows all the training data sets used in this study. The training data sets are divided into three categories. Data Set 1 is used to study the effect of temperature changes, and Data Set 2 is intended to investigate the influence of the amplitude variation of the input force. The control limits of the control charts are first constructed using all the data in Data Sets 1 and 2. Then, the preliminary damage diagnosis is conducted for 9 different damage cases shown in Data Set 3. Finally, diagnosis tests using 40 addition test sets are carried out to assess the performance of the proposed process monitoring technique. The condition of the 40 test sets was unknown to the analysts until the

completion of the diagnosis analysis. It should be noted that the presented damage diagnosis is performed in an *unsupervised learning* mode implying that data from a damaged system is not available for training purpose [1]. This feature of the proposed study is very attractive for monitoring full-scale civil infrastructures because the collection of training data sets representing various damage states of such complex structures is typically not feasible.

For each run in Table 1, the response acceleration time series are recorded at all mass points for approximately 16 second. A sample rate of 1024 per second resulted in a Nyquist frequency 512 Hz. The measured 16385 point time series are first sampled at every 46 points yielding the freqeuncy range of 0–11 Hz. Using the order identification techniques described in Reference [2], AR(36) is shown to remove most of correlation between the residuals over time. This AR(36) is then fitted to individual time series resulting in 322 ($\approx 16385/46$ - 35) residual errors. For the X-bar and S control charts, subgroups of size n=4 are employed, and for the rest of the control charts, individual residuals are plotted (n=1).

Table 1: A list of training data sets

Data Set 1: Temperature variation (total 33 sets) (All excitation have the same amplitude, Amplitude=100)											
Random input	Temperature (C^o)										
	-10	-5	0	5	10	15	20	25	30	35	40
1	Run1	Run2	Run3	Run4	Run5	6	7	8	9	10	11
2	12	13	14	15	16	17	18	19	20	21	22
3	23	24	25	26	27	28	29	30	31	32	33

Data Set 2: Input excitation variation (total 9 sets)			
Constant Temperature (C^o)	Random Excitation		
	Amplitude =50	Amplitude =100	Amplitude =300
15	Run34	35	36
15	37	38	39
15	40	41	42

Data Set 3: Testing damage cases (total 9 sets) (All cases have the same temperature 15 C^o and the same amplitude excitation)			
Stiffness Reduction	Damage Location		
	k2	k6	k2 and k6
20%	Run43	744	58
50%	45	46	59
70%	47	48	60

Figure 4 illustrates typical control charts. The time series associated with measurement point 5 (m5) of Run 59 are used for this figure. Note that all the control charts are designed such that

approximately 99% of the observation points fall within the control limits when the system is in control. When Run 59 has 50% damage both on k2 and k6, all the control charts display statistically significant number of outliers (more than 1% of the entire points) in Figure 4. This damage diagnosis is repeated for all run cases, from Run1 to Run 100. The diagnosis results of m5 are summarized in Table 2 for selected damage cases of the blind test data. The entries in columns 2-7 show the number of outliers obtained from each control chart.

It is the authors' belief that most end users of the health monitoring system simply want to know if the system is safe or not. To deduce the system integrity from the presented outlier numbers, a decision table based on the number of outliers are established and presented in Table 3. According to this decision table, the system status is assigned to one of three groups: safe (green light), questionable (yellow light), and danger (red light). When the green light is on, the end users have a confidence that the system is in-control. If a yellow light is on, the system will be still functional but a further detailed diagnosis or visual inspection is strongly recommended. Finally, a red light indicates that the system should be shut down immediately, and the operation of the system should not be resumed until assignable causes are found and regulated.

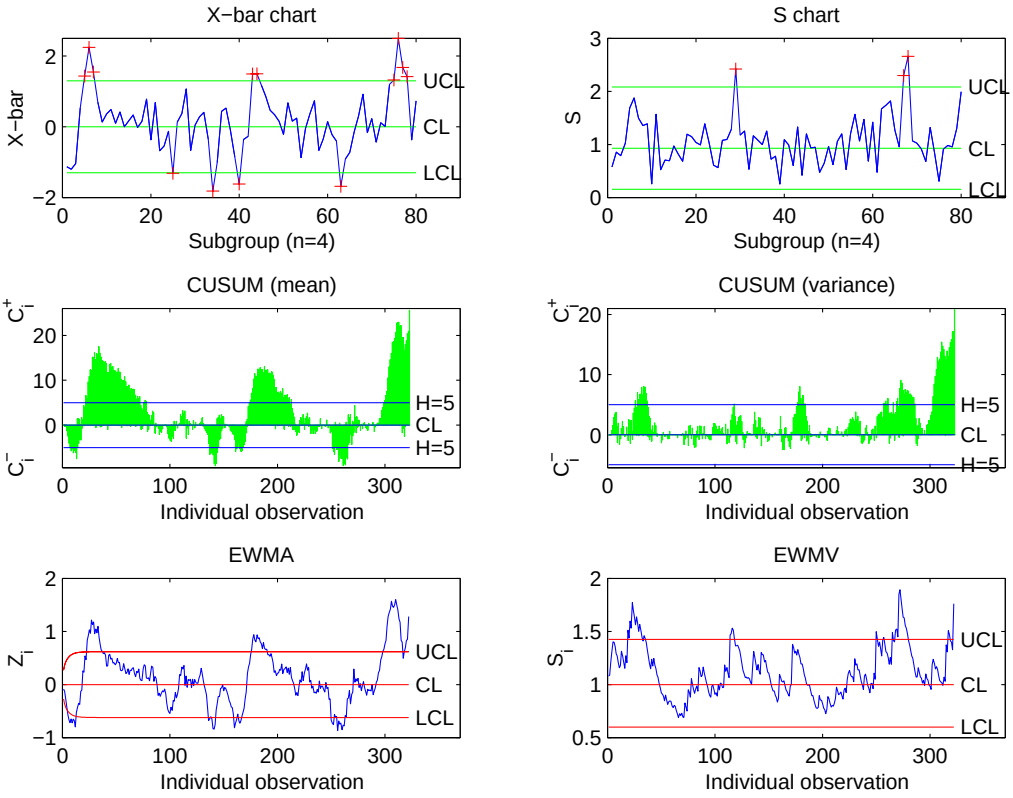

Figure 4: An example of control chart analyses

Table 2: Number of outliers and diagnosis results obtained from m5

Run #	Xchart	Schart	CUSUM (mean)	CUSUM (variance)	EWMA	EWMV	Result
63	**9**	**14**	**62**	**298**	**19**	**189**	**3**
72	**6**	**11**	**9**	**236**	**1**	**116**	**3**
76	**28**	**23**	**328**	**318**	**167**	**261**	**3**
79	**1**	**8**	**4**	**176**	**0**	**68**	**2**
80	**10**	**5**	**14**	**17**	**3**	**20**	**2**
84	**2**	**5**	**0**	**12**	**2**	**13**	**2**
87	**18**	**9**	**313**	**289**	**160**	**106**	**3**
90	**2**	**8**	**19**	**139**	**3**	**80**	**2**
93	**9**	**4**	**31**	**19**	**2**	**15**	**2**

For example, if 10, 5, 14, 17, 3, 20, and 2 number of outliers are observed for the X-bar, S,.., EWMV control charts of Run 80, then red (3), yellow (2), red (3), yellow (2), green (1), red (3) lights are assigned to the X-bar, S,.., EWMV control charts, respectively, based on the decision criteria in Table 3. That is, based on the number of outliers (n_o), the diagnosis result of each control chart is assigned to one of the following three lights: green (1), yellow (2), and red (3) lights. If we define n_L as the sum of all the numerical values of lights from each control chart, the total number of lights for this example becomes n_L=3+2+3+2+1+3=14. Because $9 < n_L < 14$, a yellow light is assigned to this measurement point based on the criteria shown in the last column of Table 3. Note that the specific values of the decision criteria are assigned in a rather heuristic manner by observing the numbers of outlier from the training data sets. A further study is needed to establish a systematic way of constructing such a decision table.

Table 3: Decision table for individual control chart

Light	Xchart (m=80)	Schart (m=80)	CUSUMX (m=322)	CUSUMS (m=322)	EWMA (m=322)	EWMV (m=322)	Results
Red=3	n_o>5	n_o>5	n_o>10	n_o>20	n_o>7	n_o>10	n_L>14
Yellow =2	n_o>2	n_o>2	n_o>4	n_o>7	n_o>4	n_o>5	n_L>9
Green=1	else	else	else	else	Else	else	else

Although all the results are not presented in this paper, the aforementioned procedure is repeated for all ten measurement points. Only the final diagnosis of each measurement point is summarized for selected damage cases in Table 4. The last column of Table 4 shows the final decision regarding the system states combining all the diagnosis results form the ten measurement points. A red light is assigned to the

system when there are more than one red light or five yellow lights from the ten measurement points. If there are less than three yellow lights for the run case of interest, a green light is assigned to the final diagnosis results. A yellow light is assigned to all the other cases.

Table 5 compares the diagnosis results analyzed by the proposed approach with the actual damage scenarios. As mentioned earlier, the actual damage status of these blind test data was not revealed to the analysts until the diagnosis analysis is completed. The 40 runs of the blind test data consist of 16 damage cases and 24 undamaged cases with various temperatures and excitation force amplitudes. Several conclusions are made based on the observation of Table 5: (1) No false-positive warning of damage is indicated out of 24 undamaged cases in spite of varying temperatures and different excitation amplitudes, and (2) out of 16 damage cases, 13 cases are successfully assigned either to red (9) or yellow (4) lights. The remaining undetected 3 damage cases have relatively small amount of damage with 10%-20% stiffness reductions. Note that because the primary objective of this study is to identify the existence of damage, the final decision regarding the system integrity is presented in terms of only three categories: green, yellow, and red lights. The localization and quantification of damage is beyond the scope of this study.

Table 4: Final diagnosis results

Run	M1	m2	m3	m4	m5	m6	m7	m8	m9	m10	Final
61	**2**	**2**	**2**	**1**	**1**	**1**	**1**	**1**	**1**	**2**	**2**
63	**3**	**3**	**3**	**3**	**3**	**3**	**3**	**3**	**1**	**3**	**3**
66	**3**	**3**	**2**	**1**	**1**	**1**	**1**	**1**	**1**	**1**	**3**
68	**3**	**2**	**1**	**1**	**1**	**2**	**1**	**1**	**2**	**1**	**2**
72	**2**	**2**	**2**	**2**	**3**	**3**	**3**	**2**	**1**	**1**	**3**
76	**2**	**2**	**2**	**3**	**3**	**3**	**2**	**3**	**1**	**2**	**3**
79	**2**	**2**	**2**	**2**	**2**	**2**	**2**	**2**	**1**	**1**	**3**
80	**1**	**1**	**1**	**1**	**2**	**2**	**3**	**1**	**1**	**1**	**2**
84	**2**	**3**	**3**	**3**	**2**	**2**	**1**	**1**	**1**	**1**	**3**
87	**2**	**2**	**2**	**3**	**3**	**2**	**2**	**1**	**1**	**1**	**3**
90	**3**	**3**	**2**	**2**	**2**	**3**	**3**	**1**	**1**	**1**	**3**
93	**3**	**3**	**3**	**3**	**2**	**3**	**3**	**3**	**1**	**2**	**3**
99	**2**	**2**	**2**	**1**	**1**	**1**	**1**	**1**	**1**	**1**	**2**

Table 5: Comparison of diagnosis results and actual damage status for the blind test data

Run	**61**	62	**63**	64	65	**66**	67	**68**	69	70
T (C^{o})	**4**	39	**28**	23	12	**28**	23	**4**	31	27
Input	**95**	190	**220**	75	190	**95**	280	**220**	190	190
Diagnosis	**2**	1	**3**	1	1	**3**	1	**2**	1	1
Actual	**k4**	No	**k3,9**	No	No	**k2**	No	**k1,7**	No	No

Damage	**20%**		**70%**			**45%**		**15%**		
Run	71	**72**	73	**74**	75	**76**	77	78	**79**	**80**
T (C°)	23	**28**	-8	**4**	23	**28**	27	23	**4**	**28**
Input	75	**95**	190	**95**	280	**220**	190	125	**95**	**95**
Diagnosis	1	**3**	1	**1**	1	**3**	1	1	**3**	**2**
Actual Damage	No	**k8 80%**	No	**k10 20%**	No	**k6 70%**	No	No	**k10 60%**	**k8 45%**
Run	81	82	83	**84**	85	86	**87**	88	89	**90**
T (C°)	4	39	28	**23**	12	28	**23**	4	31	**27**
Input	190	280	190	**95**	190	190	**220**	125	190	**220**
Diagnosis	1	1	1	**3**	1	1	**3**	1	1	**3**
Actual Damage	No	No	No	**k4 60%**	No	No	**k5 70%**	No	No	**k1,7 50%**
Run	91	92	**93**	94	95	96	**97**	98	**99**	**100**
T (C°)	23	31	**28**	39	23	-8	**4**	12	**28**	**28**
Input	75	190	**95**	190	125	190	**220**	190	**220**	**220**
Diagnosis	1	1	**3**	1	1	1	**1**	1	**2**	**1**
Actual Damage	No	No	**k2 80%**	No	No	No	**k5 15%**	No	**k3,9 10%**	**k6 10%**

4. SUMMARY AND DISCUSSIONS

The structural health monitoring is described in the context of a statistical process control paradigm. First, an auto-regressive prediction model is fitted to the time series obtained from the intact structure so as to estimate coefficients of the prediction model. The residual errors between the measured time series and the predictions from the auto-regressive model are computed for each damage case. These residual errors are defined as features for the subsequent control chart analysis. Next, the control charts are constructed using the features corresponding to the initial structure in control. After the construction of the control limits, the number of outliers, which are charted points outside the control limits, is counted for each control chart. Finally, the system status is assigned into one of three lights, green (safe), yellow (questionable), and red (danger), based on the number of outliers. Damage diagnosis with the 40 blind test data demonstrated that the statistical control chart successfully identified most of stiffness reduction (13 cases out of 16 damage cases) without any false-positive indication of damage for all the examined 24 undamaged cases.

The presented control chart analysis has several advantages over most of existing damage diagnosis techniques in that (1) the presented approach does not require the construction of any complicated analytical model nor extensive computation power, (2) the environmental and operational conditions are explicitly considered so that the effect of damage on the vibration response could be discriminated from these effects, and (3) the construction of the control charts solely relies on the vibration data obtained from the undamaged

structure without requiring data collection from various damage status. These features make the proposed approach very attractive for the development of an automated monitoring system for *in-situ* complex structures operating in adverse environments. However, the presented approach only indicates the existence of damage and does not locate the damage.

ACKNOWLEDGEMENT

The funding for this work has come from the Department of Energy's Enhanced Surveillance Program and a cooperative research and development agreement (CRADA) with Kinemetrics Corporation, Pasadena, California. The Department of Energy has funded the authors' participation in this CRADA. The authors also would like to thank Dr. Phillip J. Cornwell of Rose-Hulman Institute of Technology and Jason S. McIlhaney of California Institute of Technology for generating the numerical test data.

REFERENCES

[1] Bishop, C. M., *Neural Networks for Pattern Recognition* Oxford University Press, 1995.

[2] Box, G. E. P., Jenkins, G. M., and Reinsel, G. C., *Time Series Analysis: Forecasting and Control*, 3 ed. Prentice Hall, 1994.

[3] Hawkins, D. M., "A CUSUM for a scale parameter," *Journal of Quality Technology*, vol. 13, 1981.

[4] Lucas, J. M. and Saccucci, M. S., "Exponentially weighted moving average control schemes: properties and enhancements," *Technometrics*, vol. 32, 1990.

[5] MacGregor, J. F. and Harris, T. J., "The exponentially weighted moving variance," *Journal of Quality Control Technology*, vol. 25, 1999.

[6] Montgomery, D. C., *Introduction to Statistical Quality Control* John Wiley and Sons Inc., 1997.

[7] Roberts, S. W., "Control chart tests based on geometric moving averages," *Technometrics*, vol. 1, 1959.